Physical Characteristics and Controlling Factors of Coal Gas Reservoir in Pingdingshan No. 10 Coal Mine

Dejie Zhou , Juan Wang * , Baoyu Wang , Di Gao , Junjie Zhao

Posted Date: 30 October 2023

doi: 10.20944/preprints202310.1832.v1

Keywords: Pingdingshan No. 10 coal mine; Coalbed gas reservoir; pore-fracture characteristics; adsorption characteristics; gas-bearing properties

Article

Physical Characteristics and Controlling Factors of Coal Gas Reservoir in Pingdingshan No. 10 Coal Mine

Dejie Zhou [1], Juan Wang [1,2,*], Baoyu Wang [1], Di Gao [1] and Junjie Zhao [1]

[1] School of Resources and Environment, Henan Polytechnic University, Jiaozuo 454003, China
[2] Collaborative Innovation Center of Coal Work Safety and Clean High Efficiency Utilization, Henan Polytechnic University, Jiaozuo 454003, China
* Correspondence: wangjuan@hpu.edu.cn

Abstract: The physical properties of coal reservoirs are the main restrictions to exploration and development of CBM. The study of the physical characteristics of coal reservoirs and their controlling factors is of great significance to the safe and efficient development and utilization of CBM resources in the mining area. The Pingdingshan No. 10 coal mine was chosen for this study because of its better gas production effect at the test wells. The reservoir properties of the main coal seams of the No. 10 coal mine were tested and analyzed to comprehensively evaluate the reservoir properties, the physical characteristics and controlling factors of coal reservoir in Pingdingshan No. 10 coal mine were studied. The results indicated that (1) The gas content and methane purity of the No. 4 coal seam were significantly higher than the No. 2 seam, and therefore they have better development potential than the No. 2 seam; (2) The average adsorption time of the No. 2 coal seam was less than that of the No. 4 seam, making it easier to reach the peak production capacity of CBM wells in the short term, but was not conducive to long-term stable production of CBM. The Langmuir volume of the No. 2 coal seam samples was significantly greater than for the No. 4 coal seam; however, the No. 4 coal seam contains about three times the amount of gas in the No. 2 seam; (3) All three coal seams have high porosity, which was favorable for large amounts of CBM adsorption and storage. Micropores predominate, transitional pores were less frequent, and a few mesopores occur; macropores were the least common. Samples from the No. 4 seam contained the highest proportion of micropores; (4) Organic pores were common in the all coal samples, with pore diameters not more than 30 μm, mainly concentrated between 50.5 and 1000 nm. Microfractures with aperture less than 70 nm were relatively frequent, mainly in the 50–65 nm range. A large number of the nanoscale microfractures were curved or jagged; (5) Fractures in the No. 2 and No. 4 coal seam samples with widths of 50 nm to 20 μm were more developed, and many were filled with kaolinite, quartz and other minerals; (6) The samples contained mostly layered silicate minerals (kaolinite), with hard granular minerals (quartz) next, and a very small quantity of iron-type minerals such as siderite and pyrite in dendritic form. The results of this study can provide a reference basis for the large-scale development and utilization of subsequent CBM wells.

Keywords: Pingdingshan No. 10 coal mine; Coalbed gas reservoir; pore-fracture characteristics; adsorption characteristics; gas-bearing properties

1. Introduction

Coalbed methane (CBM) is an unconventional natural gas whose main component is methane, which plays a very important role in the energy field [1–3]. The growth of China's CBM industry has slowed in recent years, and there is an urgent need to stimulate its development by carrying out research programs [4–7]. The study of the physical properties of coal reservoirs plays a pivotal role in the development of coalbed methane industry, and the efficient exploration and development of coalbed methane has received wide attention. Therefore, it is of great significance to deeply

 doi:10.20944/preprints202310.1832.v1

understand the characteristics of coal reservoirs and guide the efficient development of coalbed methane reservoirs [8,9]. Great achievements have been made in the study of coal reservoir, but the systematic study on the physical properties of coal reservoir in Pingdingshan mining area is relatively lacking.

The physical characteristics of coal reservoirs include porosity, permeability, methane adsorption capacity and gas content [10–12]. The permeability is closely related to the buried depth. With the increase of the buried depth, the effective stress increases and the permeability decreases exponentially [13]. Gas content (i.e., in situ gas content, residual gas content, free gas content, and adsorbed gas content) is rarely used in measurement and estimation [14,15]. Mainly field methods were used in the present study to test the gas content of three coal seam sections for comparative analysis. Quantitative pore and fracture analysis is an important means of characterizing the physical properties of coal reservoirs. Coal is usually described as a dual pore system, with fractures being the main contributor to fluid flow [16,17]. Gas flow in the pore space is in two stages: gas adsorbed in the coal matrix diffuses into the coal seam fractures, then flows predominantly through the fracture network [18–20]. Coal matrix pores are categorized by pore size; most pores are too small to be resolved by micro-CT scanning images, so in this study scanning electron microscopy (SEM) was used to resolve nanometer-sized pores and obtain information about the surface morphology and composition of the samples [21]. The pore structure and pore size distribution of the coal matrix were measured by high-pressure mercury injection (HPMI). It is generally believed that coalbed gas adsorption is physical adsorption, there is an adsorption site on the surface of coal, and fluid molecules are bound by van der Waals force [22]. The fitted expression of isothermal adsorption experimental data was used to calculate the adsorbed gas content, and showed that the rate of adsorbed gas content increases rapidly at low pressure, then decreases significantly when the pressure reaches a certain value; that is, greater adsorptive capacity occurs at high reservoir pressures [23–25]. The mineralogical composition of the coal also has a strong influence on the gas content of the coal. X-ray diffraction (XRD) was used to quickly analyze the specific types and relative content of minerals [26].

The subjects of this study were the main mining coal seams of No. 10 coal mine at different depths: No. II1, No. IV2 and No. IV3 seams. The geological and coal seam data for No. 10 coal mine were collected, the microscopic pore fracture surface morphology of each sample was observed by SEM and HPMI, the porosity of the samples was measured, and the pore and fracture properties of the samples summarized. Finally, the influence of different factors on the gas content of the three main coal seams in the area was revealed for the reservoir materials. The purpose of this study was to provide a scientific reference for the exploration and development potential of CBM in the Pingdingshan region.

2. Geological conditions and background of mining area

2.1. Geological condition

The Pingdingshan mining area is located at the front edge of the NW-oriented large-scale retrograde thrust belt in the Xiaoxiong tectonic zone at the southern edge of the North China Plate, lying within the transition area between the North China Plateau and the Qinling Fold Belt. The mining area is an independent uplifted fault block surrounded by depressions, evidenced by NW-striking fractures and folds. The main tectonic structure of the whole mining area is the Likou syncline, with the No. 10 coal mine located on its NE flank. In general, the No. 10 coal mine is a tectonomonocline dipping NNE. The basic tectonic forms are the No. 10 coal mine syncline and the Guozhuang anticline developed in the dip direction. The faults are mainly the original No. 11 Mine reverse fault and the Niuzhuang reverse fault between the axes of the Guozhuang anticline and the No. 10 coal mine syncline. The axial direction and strike of the folds and faults are basically parallel, indicative of the clearly regular spread of folds and faults in the NW direction. The tectonic subdivision of the Pingdingshan mining area is shown in Figure 1.

Preprints (www.preprints.org) | NOT PEER-REVIEWED | Posted: 30 October 2023 doi:10.20944/preprints202310.1832.v1

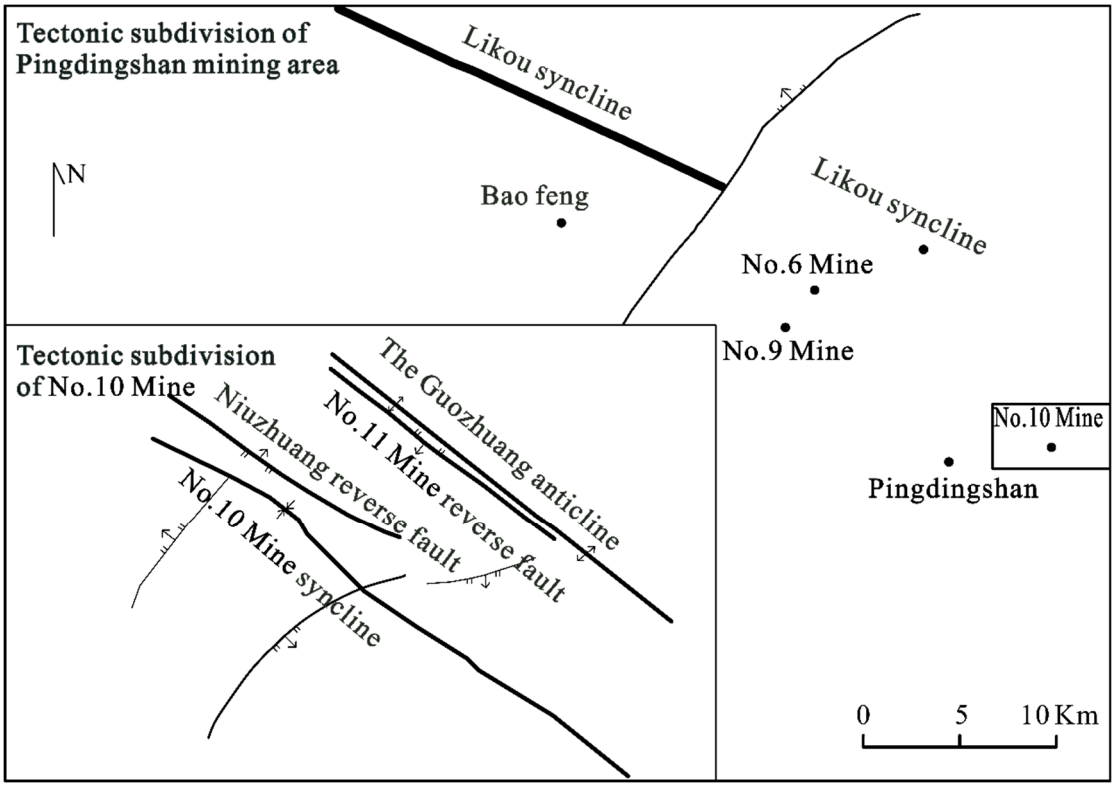

Figure 1. The tectonic subdivision of the Pingdingshan mining area (Own work).

The Pingdingshan mining area is part of the North China stratigraphic area. The ages of these strata, from oldest to most recent, are Neoproterozoic, Cambrian, Carboniferous, Permian and Quaternary, of which the Carboniferous and Permian are the coal-bearing strata. The No. 10 coal mine is located in the east of Pingdingshan mining area; the coal-bearing strata are the Upper Carboniferous Taiyuan Formation (C2t), the early Permian Shanxi Formation (P1s) and Shihezi Formation (P1x), and the late Permian Upper Shihezi Formation (P2s), totalling 4l seams. The total thickness of the seams is 36 m. The coal-bearing proportion is 4.62%, with the Shanxi Formation and late Shihezi Formation being the main coal-bearing strata.

2.2. Background

Coal is composed of matrix, fractures, pores and minerals, etc. The coal matrix also known as coal bedrock, is a coal block divided by cleat, and CBM is mainly stored in coal bedrock by adsorption; Fracture is mainly the channel of CBM migration, and pore is mainly the occurrence space of CBM; Minerals are naturally occurring uniformly ordered solids that are an important part of coal; Ashed at low temperatures is to burn the sample at low temperature, so that it can be converted into ashes, and finally retain the inorganic components in the sample; Normalization is to limit the data to be processed to a certain range after processing through a certain algorithm, for the convenience of data processing later; "Sweet spot" refers to the area where CBM is enriched, while engineering sweet spot is based on geological sweet spot, and the CBM in this area is easy to be fractured.

3. Samples and experimental methods

3.1. Samples

Coal samples were from No. II1 seam in the Shanxi Formation, and Nos. IV2 and IV3 seams in the Lower Shihezi Formation. No. II1 coal seam is located in the lower part of the Shanxi Formation. The average thickness of the seam is about 4 m; its simple structure is derived from the bay–tidal flat sedimentary system, and it is quite stable. No. IV2 seam is in the lower part of four coal segments of the Lower Shihezi Formation, with an average thickness of 2.64 m, and is also quite stable. No. IV3

 doi:10.20944/preprints202310.1832.v1

seam, from a lower delta plain depositional environment, is 0.95 m thick and is only locally recoverable. The direct roof of the three seams is a dark gray sandy mudstone, with a mudstone floor. A total of five fresh coal samples were collected for this study from the underground face of the No. 10 Mine. After the samples were pretreated, they were subjected to HPMI, SEM, methane isothermal adsorption, gas content and XRD tests.

3.2. Petrographic characteristics

Macrolithotypes of coal: SK21 coal is predominantly semi-bright, black, glassy, with black-brown streaks. Fracturing is evident at a density of about 9 cracks every 5 cm. The macrolithotype of SK42 and SK43 is dominated by semi-dark to semi-glossy coals, with black color, glassy luster and 1–2° hardness, and smooth fractures. The structure is generally banded, blocky and/or laminated. The macroscopic characteristics of SK21, SK42 and SK43 are shown in Figure 2.

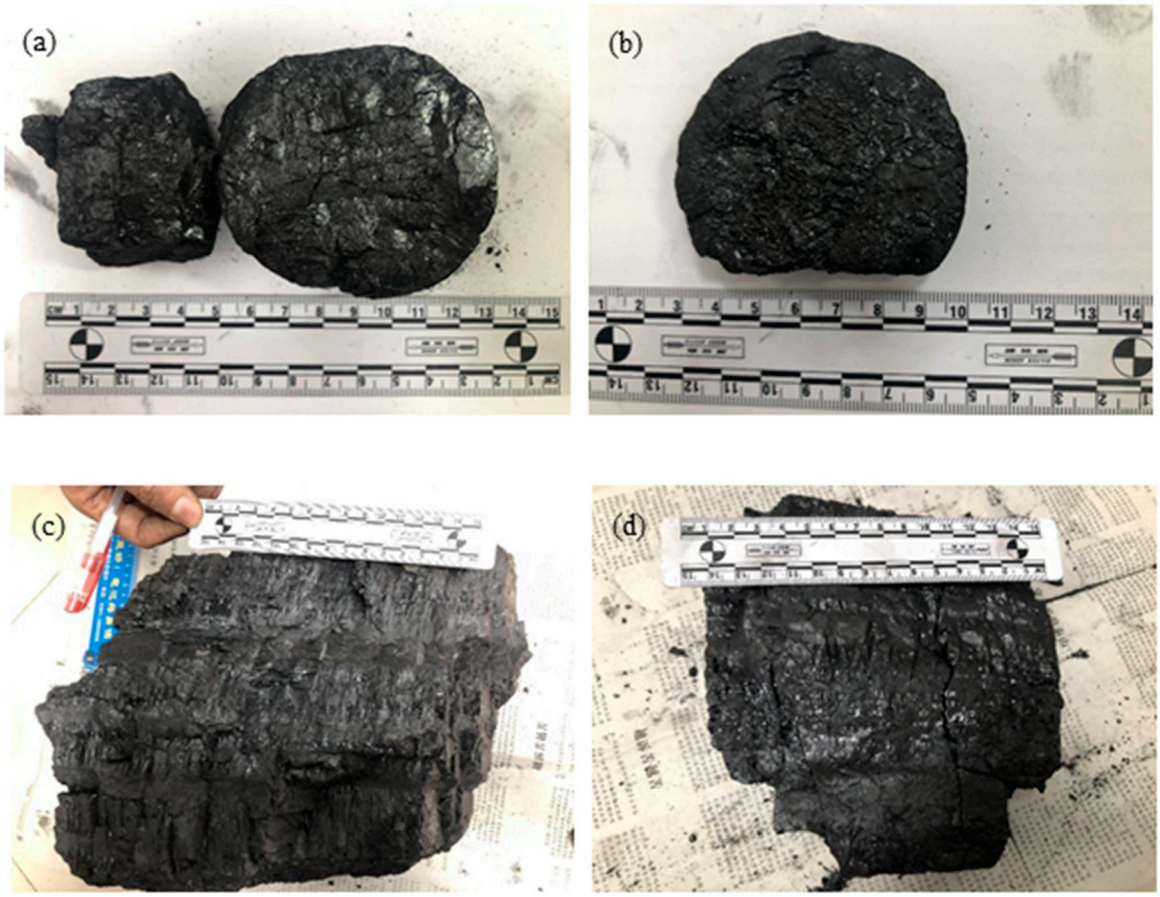

Figure 2. Macroscopic Coalstone Types of Samples SK21, SK42 and SK43 (Own work): (a). SK21 semi-dark coal; (b). SK21 semi-light coal; (c). SK43 semi-light coal; (d). SK42 semi-dark coal.

Microscopic characteristics of coal: In SK21 coal, organic macerals are dominated by 81.81–82.53% vitrinite (average 82.17%), mainly desmocollinite and telocollinite; 8.72–10.11% inertinite (average 9.42%), mainly fusinite and macrinite, with a small amount of semifusinite and individual micrinite and sclerotinite particles. The inorganic mineral content is 8.08–8.75% (average 8.41%) consisting mainly of clusters or bands of clay minerals, and a few fine veins of carbonate rocks.

SK42 and SK43 organic macerals are dominated by 60.94–73.38% (average 68.53%) vitrinite comprising mainly desmocollinite and telocollinite, with a small amount of vitrodetrinite. The 12.23–25.62% inertinite (average 19.42%) is dominated by macrinite, fusinite, a small amount of semifusinite and individual particles of sclerotinite, together with occasional exinite (1.56–9.04%, average 4.70%),

 doi:10.20944/preprints202310.1832.v1

mainly seen as microsporinite. The 3.90– 12.83% (average 7.35%) inorganic mineral component is dominated by bands of clay minerals (Table 1).

Table 1. Microcompositional characterization of SK21, SK42 and SK43 samples (%) (Own work).

Sample ID	Maceral			
	Vitrinite	Inertinite	Exinite	Inorganic mineral component
SK21	82.17	9.42	-	8.41
SK42#1	68.53	19.42	4.70	7.35
SK42#2	68.53	19.42	4.70	7.35
SK43#1	68.53	19.42	4.70	7.35
SK43#2	68.53	19.42	4.70	7.35

3.3. Experimental methods

3.3.1. HPMI

The HPMI of coal samples was carried out under the standard ISO 15901-1: 2016. Before testing, the coal samples were cut into 3-6 mm cubes, and 2–3 g of the sample were placed in an oven at 70-80°C for 12 h, then dried at room temperature prior to testing. HPMI was then carried out using a Mack AutoPore V9600 device, which provides a maximum mercury injection pressure of 227 MPa. The pore throat interval was determined using Washburn's equation to be 5.5 nm – 343 μm. Then semi-quantitative characterization of the pore structure parameters of the coal was determined (e.g., pore size distribution, specific surface area, pore volume, porosity, and other physical properties).

3.3.2. SEM

Observations were made using a FEI Quanta 250 FEG-SEM scanning electron microscope. Fresh surfaces of samples no larger than 1 cm × 1 cm × 1 cm were observed. To improve the electrical conductivity, the surface was coated with gold by ion beam sputter deposition for 80 s.

3.3.3. Isothermal adsorption

The Langmuir adsorption constants V_L and P_L of coal samples was carried out under the standard GB/ T19560-2008. Isothermal adsorption experiments were carried out using an intelligent analyzer coal methane adsorption tester WX-VI with a maximum pressure of 16 MPa and a constant temperature range of 20–50°C. The sample was weighed, equilibrated with water, and loaded into the isothermal adsorption sample tank. The thermostatic water bath was raised until the reference and sample tanks were all submerged. Helium was then injected at a particular pressure into the reference tube and recorded after equilibrium. Pressure opens the connected valve, allowing the gas to diffuse into the sample canister until equilibrium, and the sample volume is calculated by Boyle's law, close the valve, and then injected methane to the reference tank, repeated adsorption, until the completion of the test.

3.3.4. The coalbed methane (CBM) content

The coalbed methane (CBM) content was determined in accordance with Chinese national standard GB/T 19559-2021. Individual samples weighing 900 g were loaded into the desorption canister and tightly sealed. An Agilent 8890 gas chromatograph (GC) was used to determine the gas content of the main coal seam of No. 10 Mine, at an output pressure of 0.5–0.6 MPa.

3.3.5. XRD

Five groups of coal samples were pulverized to 200 mesh in vacuum at room temperature, then ashed at low temperatures to remove organic matter. Their mineral content was determined using a SmartLab 9kW XRD at 5–90° angles and 5–15° min^{-1} rates.

Preprints (www.preprints.org) | NOT PEER-REVIEWED | Posted: 30 October 2023 doi:10.20944/preprints202310.1832.v1

4. Results and Discussion

4.1. Adsorption characteristics of coal

Coal has strong adsorption characteristics for methane gas molecules due to van der Waals forces, as described by the Langmuir equation [27]. Stronger adsorption results in greater gas storage and content potential of coal. Therefore the methane adsorption characteristics of the coal were used to predict the potential gas-bearing resources in the study area. The adsorption of coal is mainly characterized by Langmuir volume and Langmuir pressure (PL). The isothermal adsorption experiments at 30°C of the three coal seams in No. 10 coal mine (Table 2) showed the air-dried basis Langmuir volume of SK21 was 13.82 m^3t^{-1} at PL = 0.44 MPa, and the values for SK42 and SK43 were 8.36–13.18 m^3t^{-1} at PL = 0.69–1.21 MPa. Langmuir volume was 8.36–13.18 m^3t^{-1}, and the theoretical saturated adsorption of methane by SK42 and SK43 was slightly lower than for SK21.

Table 2. Results of isothermal adsorption experiments on SK21, SK42 and SK43 samples (Own work).

Sample ID	Moisture/%	Ash /%	Air dried basis		
			Langmuir volumetric V_L/ $m^3 \cdot t^{-1}$	Langmuir pressure P_L/MPa	R^2
SK21	1.91	10.57	13.82	0.44	0.9927
SK42#1	0.93	11.67	13.18	1.07	0.9904
SK42#2	1.49	12.59	10.25	1.01	0.9935
SK43#1	0.68	23.99	9.71	1.21	0.9957
SK43#2	0.72	20.06	8.36	0.69	0.9823

The isothermal adsorption graphs for the samples are shown in Figure 3, which shows that the Langmuir equation fits the five sets of experimental data well ($R^2 > 0.98$). Of the five sets of results, SK43#1 has the poorest fit and SK43#2 has the best fit. The five curves indicate that the overall adsorption trend is basically the same, where the adsorbed amount in the low-pressure region increases rapidly up to a certain value, when the increase clearly slows and the adsorbed volume in the high-pressure region gradually tends toward saturation. When the pressure is less than 3.5 MPa, the adsorbed amount of SK43#1 under the same pressure is less than SK43#2. When the pressure reaches about 3.5 MPa, the adsorbed amount of SK43#1 and SK43#2 is equal, and then with the increase of the pressure, the adsorption capacity of SK43#1 is higher than that of SK43#2. In general, the Langmuir volume increased with increase in coal rank, consistent with the theory of higher coal rank (Ro < 4.0%), and with the higher adsorption capacity reported in previous studies [28].

Preprints (www.preprints.org) | NOT PEER-REVIEWED | Posted: 30 October 2023 doi:10.20944/preprints202310.1832.v1

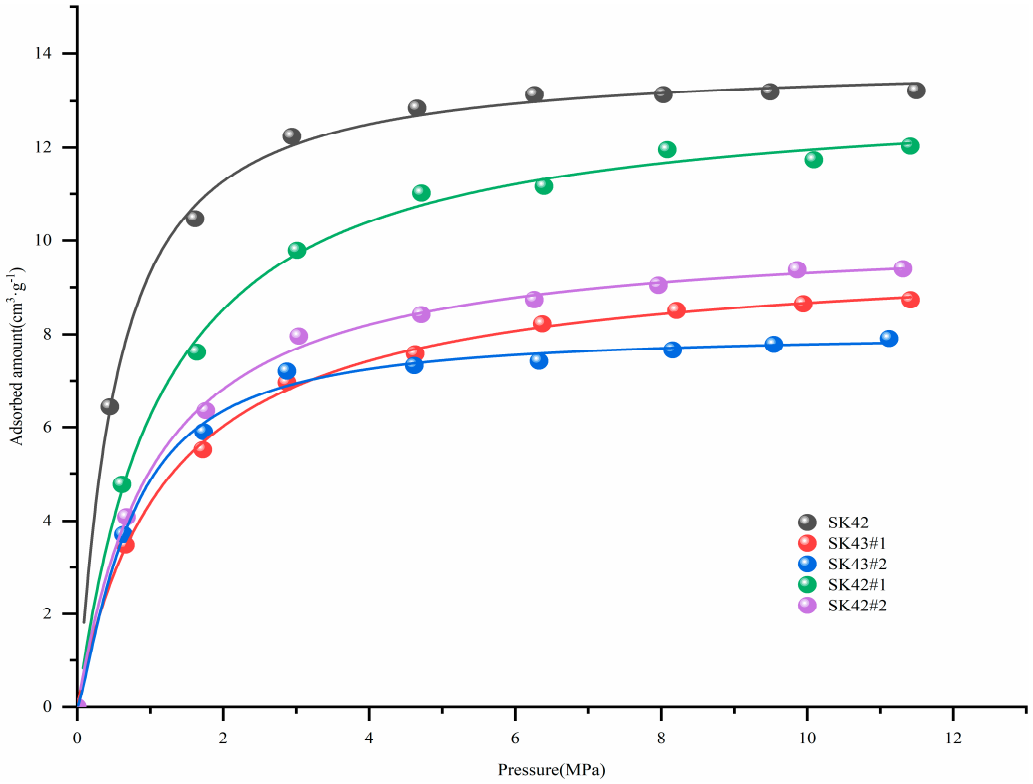

Figure 3. Isothermal adsorption profiles of SK21, SK42 and SK43 samples (Own work).

In addition to the adsorptive capacity of coal for methane, the desorption rate also affects the stability and high production of CBM wells. The desorption experimental data for SK21, SK42 and SK43 seams show that the average adsorption time of SK21 is 1.42 d, 3.5 d for SK42, and 2.73 d for SK43, the adsorption time of SK42 and SK43 is about twice that of SK21. These adsorption times are shorter than for middle-rank coal in other mines, so it follows that peak production capacity would be reached in the short term, but it is not conducive to long-term stable production of the CBM wells.

4.2. Coal seam pore and fracture characteristics

Reservoir microspace structure characterization is mainly focused on the shape, distribution, size and connectivity of pores and fractures. The pore and fracture structure is an important factor in controlling the content of CBM [29]. The microstructural characteristics of the reservoir are an important aspect of reservoir evaluation and reservoir prediction (CBM transportation, storage and seepage). Coal is often described as a dual-pore system, where pores are the spaces in the coal body that are not filled with solids, and linear fractures occur within and between the matrix blocks of the coal. The natural fracture system of coal is the main channel for CBM penetration and is a major influence on CBM output. Pores in organic matter are usually too small to provide an effective flow pathway, whereas fractures in the organic matter are believed to be the main channel for the outflow of gases. The larger cracks are the main channels, so an understanding of the pore and fracture characteristics of coal reservoirs is highly significant to the development of CBM [30,31].

4.2.1. Coal pore characteristics

In the present study, the pore structure of five groups of samples was determined by HPMI. The results shown in Table 3 and Figure 4 are summarized as follows:

• SK21 porosity was 39.34% with pore sizes ranging from 5.48 to 342 917.58 nm, of which macropores (> 1000 nm) accounted for 0.65%, mesopores (100–1000 nm) accounted for 2.36%, transitional pores (10–100 nm) accounted for 26.39%, and micropores (< 10 nm) accounted for 70.60%.

Preprints (www.preprints.org) | NOT PEER-REVIEWED | Posted: 30 October 2023 doi:10.20944/preprints202310.1832.v1

• SK42 porosity was 4.98–5.17% with pore sizes ranging from 5.48 to 342 422.90 nm, comprising 0.08% macropores, 0.23–0.34% mesopores, 26.19–30.28% transitional pores, and 69.42–73.39% micropores.

• SK43 porosity was 5.78–8.08% with pore sizes ranging from 5.48 to 342 585.98 nm, comprising 0.13–0.14% macropores, 0.36% mesopores, 20.33–26.28% transitional pores and 73.24–79.17% micropores.

Table 3. The pore structure of SK21, SK42 and SK43 samples (Own work).

Sample ID	Macropore（>1000nm）	Mesopore（100-1000）	Transitional pore（10-100）	Micropore（<10）
SK21	0.65%	2.36%	26.39%	70.60%
SK42#1	0.08%	0.23%	30.28%	69.42%
SK42#2	0.08%	0.34%	26.19%	73.39%
SK43#1	0.14%	0.36%	20.33%	79.17%
SK43#2	0.13%	0.36%	26.28%	73.24%

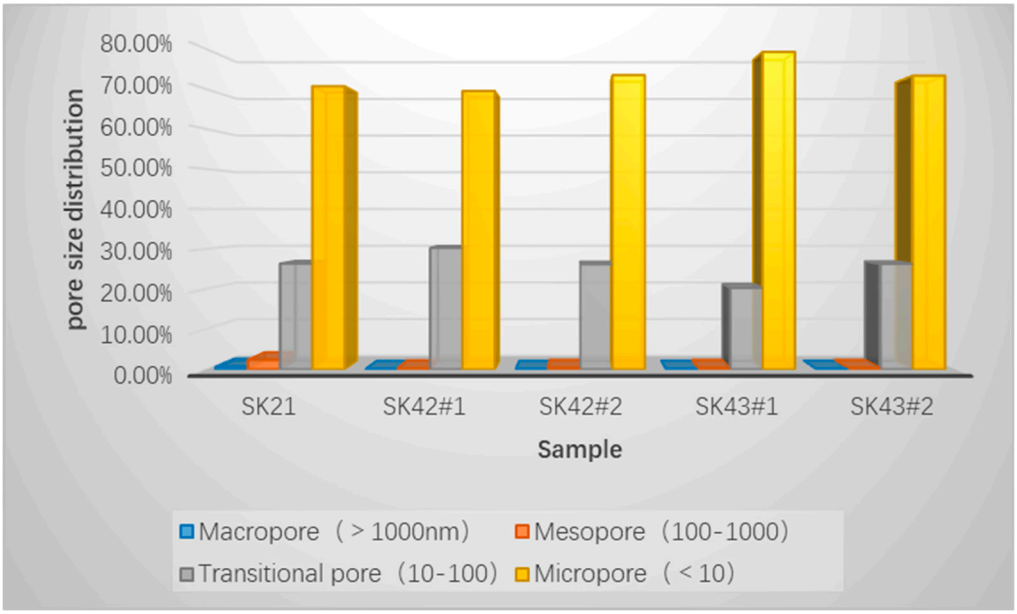

Figure 4. The pore structure of SK21, SK42 and SK43 samples (Own work).

It can be seen that the porosity of the five groups of coal samples was high, with micropores dominating, transitional pores next, a few mesopores, and the least developed were micropores, which is favorable for the adsorption and storage of large amounts of CBM. The porosity of SK21 is about 6 times that of SK42 and SK43, Of the five groups, the proportion of micropores in SK42 and SK43 is highest, with very small proportions of macropores and mesopores.

The SEM technique enables visualization of the morphology and distribution of pores and fractures in coal; although macropores, mesopores and micropores all occur in the coal matrix, it is believed that micropores are the main site of adsorbed methane [29]. The size and number of pores and fractures in coal are directly related to porosity and seepage [32]. The pores in coal are categorized into three main groups: organic-matter pores, mineral pores and microfractures. Organic-matter pores are formed within clusters of organic matter or following organic-matter hydrocarbon generation due to volume reduction; they display smooth surfaces and relatively individual and uniform arrangements. Organic-matter pores play an important role in controlling coal porosity and gas content, and are an important part of the pore system of dense coal reservoirs. Organic-matter pores are classified into nanopores (diameter < 0.75 μm) and micropores (diameter > 0.75 μm) [33,34]. Organic pores of the coal samples were more highly developed in the samples studied here, with pore diameters not exceeding 30 μm, and mainly 50.5–1000 nm, usually found in telocollinite (Figure

Preprints (www.preprints.org) | NOT PEER-REVIEWED | Posted: 30 October 2023 doi:10.20944/preprints202310.1832.v1

5a,b) and plant cell cavities (Figure 5c–f). Most of the cell lumen pores were filled with minerals (Figure 5c,d), predominantly kaolinite. A few cell lumen pores were cut longitudinally (Figure 5f), and gas–liquid inclusion pores were observed (Figure 5e). The shape of pores containing a gas or liquid inclusion is very similar to pores containing organic matter (i.e., round base, smooth pore wall, distributed in a line or group). This type of pore is due to gas or liquid remaining in the minerals after the pore was emptied [35].

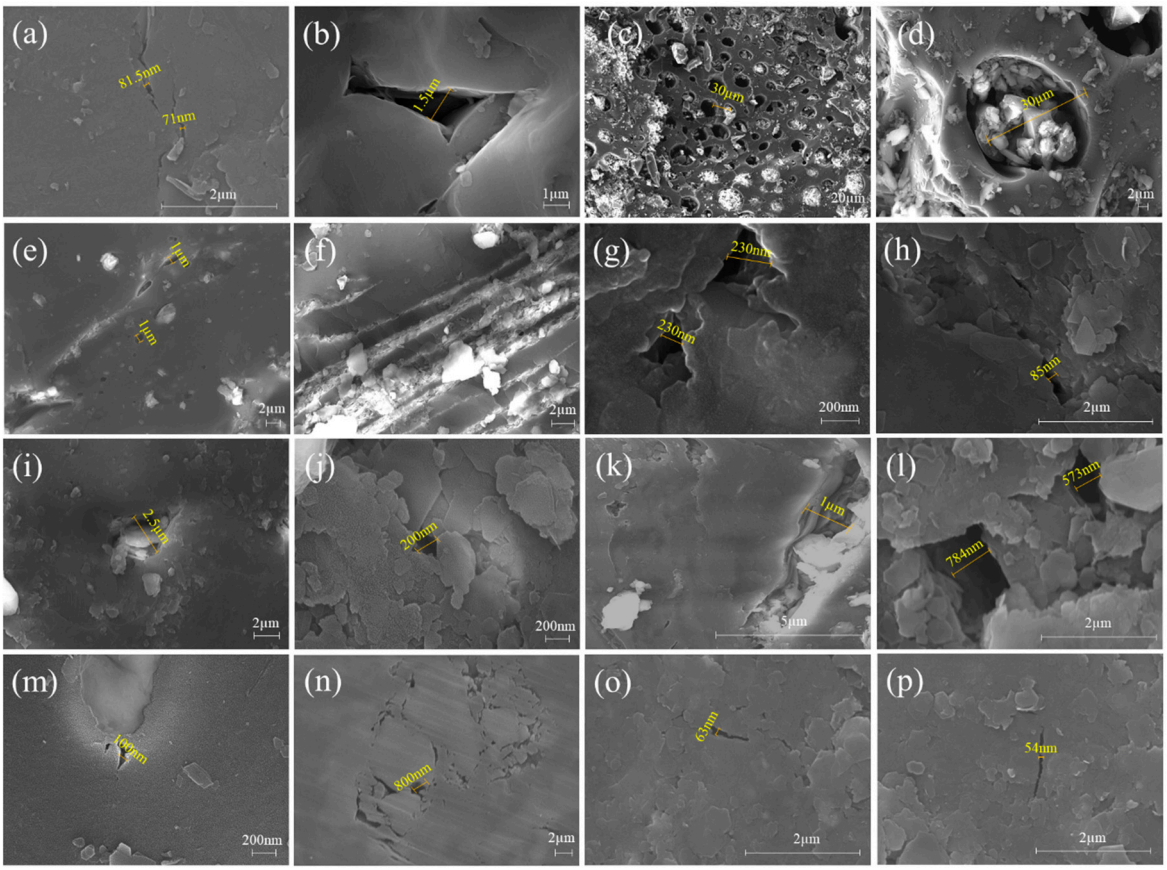

Figure 5. SEM pore images of SK21, SK42 and SK43 samples (Own work). (a) organic matter pore, SEI imaging, Sample SK42; (b) organic matter pore, SEI imaging, Sample SK42; (c) cell lumen pore, SEI imaging, Sample SK42; (d) cell lumen pore and mineral fill, SEI imaging, Sample SK42; (e) gas-liquid inclusion pore, SEI imaging. Sample SK42; (f) longitudinal cut cell lumen pore, SEI imaging Sample SK42; (g) intergranular pore, SEI imaging, Sample SK21; (h) intergranular pore, SEI imaging, Smple SK42; (i) intergranular pore, clay, SEI imaging, Sample SK43; (j) intergranular pore, clay, SEI imaging, Sample SK43; (k) intragranular dissolved pore, SEI imaging, Sample SK43; (l) intergranular pore, clay, SEI imaging SK42 sample; (m) intercrystal pore, SEI imaging, SK43 sample; (n) intragranular pore, SEI imaging, SK43 sample; (o) nanoscale microfractures, SEI imaging, SK42 sample; (p) nanoscale microfractures, SEI imaging, SK42 sample.

Inorganic mineral pores are mainly intergranular in clay minerals, rich in mainly clay minerals, together with small amounts of pyrite, calcite, dolomite, quartz, gypsum and apatite. They occur between different mineral particles, in minerals within a single particle, or between mineral crystals of the same type. Pores in organic matter and minerals are different in size, depending to their location. They may further be intergranular and intragranular holes, intercrystal pores, interlayer holes, and in organic matter and minerals between pores. Depending on the mineral type and contact relationship, intergranular pores are mainly triangular and polygonal with concave and uneven edges, and have better connectivity. Pore diameters occur mainly in the 37–2142 nm range [36], and a large number of dissolved and eroded detrital particles are present (Figure 5g–j,l). In

 doi:10.20944/preprints202310.1832.v1

addition, it was observed that a significant portion of the samples contained intergranular pores with clay mineral infill, as shown in Figure 5i. Intragranular dissolution pores were observed in feldspars and clasts, mainly banded (Figure 5k). Intercrystal pores, mainly occurring in pyrite (Figure 5m), are small (diameters ranging from 10s to 100s nm) and poorly connected, and therefore contribute little to reservoir physical properties [37].

In this study, pores between particles of different mineral types, between particles of the same mineral type, and between organic matter and mineral particles are all categorized as intergranular pores. Pores within a single mineral particle are classed as intragranular pores (Figure 5n). Most current pore classifications regard pores between clay mineral lamellae as intergranular pores, and pores between pyrite crystals are classed as intragranular pores [38]. Interlayer pores are wedge-shaped, irregular, and reticulated in a number of cases, with pore diameters from tens of nanometers to micrometers, found for example in kaolinite, illite and other lamellar clay minerals; interlayer pores were not found in the coal samples.

The morphology and scale of microfractures differ greatly between organic pores and inorganic mineral pores. Microfractures a few micrometers wide, a few millimeters long, or a few millimeters high are difficult to see without the aid of a microscope [39]. They are important channels for shale gas output and, since they bridge microscopic pores and macroscopic fractures, facilitate CBM storage and seepage [41]. Microfractures were common in the coal samples from No. 10 Mine and most were extensive and open, affording strong connectivity. Aperture is mostly < 70 nm, mainly concentrated in the 50–65 nm range. SEM observations showed large numbers of curved or jagged nanoscale microfractures (Figure 5o,p), most of them open, which is conducive to the transportation of natural gas. The porosity of the coal makes only a limited contribution to the reservoir, but it has a strong effect on improving reservoir seepage potential.

4.2.2. Coal fracture characterization

Fractures in coal are the main channels for fluid transportation and output, and they play a very important role in the effective porosity and permeability of coal reservoirs [40]. Fractures in coal are categorized as macroscopic and microscopic, depending on whether they are visible to the naked eye or can only be seen by SEM. The fracture morphology is complex and varied, from curved and straight shapes, open and closed fractures, most of which are nearly linear, and some are X-type conjugate fractures. SK21 coal is lumpy, with many fractures several 10s of micrometers wide (1.8 fractures per cm on average).

SK42 and SK43 coal is fractured with a broken grain structure, and the fractures are highly developed. The width of the fractures is 60 nm to 20 μm as observed by SEM; many are filled with minerals such as kaolinite and quartz. The fracture groups are parallel, intersecting or dendritic, most either filled with minerals or closed and unfilled. The fractures in the samples were classified as either filled or open, based on the relationship between the width of open fractures and CBM production [42]; that is, greater width of open fractures provides a better channel for CBM transportation, but filled fractures prevent CBM production.

Filled fractures: Clay mineral was the most common infill in the five groups of coal samples observed by SEM, with different morphologies. Most of the fractures were confined to a certain size range, with spacing between 10 and 20 μm, as in the case of the X-type conjugate fractures (Figure 6a), while others had small or even nanometer spacing (50–800 nm), as in the case of the dendritic fracture clusters (Figure 6b) where the minimum spacing was up to 50 nm; some intersect (Figure 6c), while others are parallel (Figure 6d). Most of the fractures were filled with granular and massive minerals (Figure 6a,b).

Preprints (www.preprints.org) | NOT PEER-REVIEWED | Posted: 30 October 2023 doi:10.20944/preprints202310.1832.v1

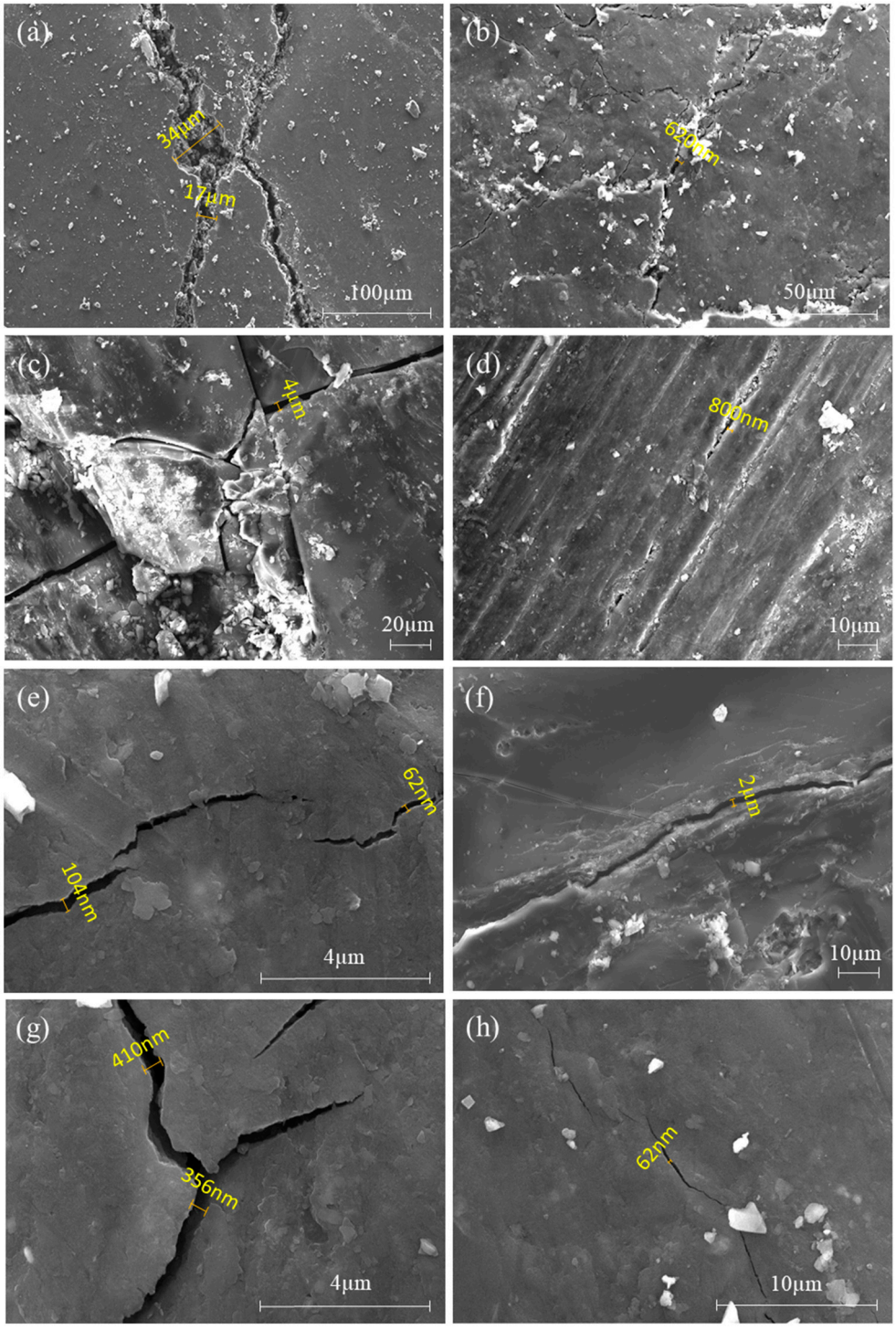

Figure 6. SEM fracture images of SK21, SK42 and SK43 samples (Own work). (a) "X" type conjugate fracture, clay mineral, SEI image, SK21 sample; (b) dendritic fracture cluster, clay minerals, SEI image, SK21 sample; (c) intersecting fracture, SEI image, SK43 sample; (d) parallel fracture, SEI image, SK21 sample; (e) geese aligned fracture, SEI image, SK21 sample; (f) straight shaped fracture, SEI image, SK42 sample; (g) approximately right-angled intersecting fracture, SEI image, SK21 sample; (h) geese aligned fracture, SEI image, SK21 sample.

Open fractures: Open fractures are usually simple in form, often occurring in a single location, and extending from one hundred to several hundreds in one place. Most of the fracture pores are straight (Figure 6f), some intersect at approximately right angles (Figure 6g), and some are similar to

Preprints (www.preprints.org) | NOT PEER-REVIEWED | Posted: 30 October 2023 doi:10.20944/preprints202310.1832.v1

echelon permutations (Figure 6h). Aperture in the samples were observed to be no larger than 2 μm, with the smallest averaging 62 nm.

4.3. Mineral composition of coal

Coal minerals consist of dispersed crystalline mineral particles, coarsely crystallized minerals, and non-crystalline inorganic elements. XRD technology quickly identifies specific mineral types and accurately names fine-grained minerals (Table 4). The main minerals in SK21 are kaolinite, followed by quartz and calcite; SK42#1 contains a large amount of kaolinite, followed by calcite and a very small amount of iron dolomite; SK42#2 contains kaolinite, followed by a large amount of quartz, a very small amount of siderite and iron dolomite; and SK43#1 and SK43#2 contain quartz and kaolinite and a very small amount of anatase, with a small amount of pyrite in SK43#2. Combined with the SEM results (Figure 5 h–m, o), it is seen that flake silicate minerals (kaolinite) were found in most of the samples, with hard-grained minerals (quartz) second only to kaolinite, and that they contain a very small amount of iron-type minerals such as siderite and pyrite in dendritic form [43].

Table 4. XRD results of SK21, SK42 and SK43 samples **(Own work).**

Sample ID	Quartz	Kaolinite	Calcite	Siderite	Dolomite	Pyrite	Anatase	Muscovite
SK21	15.2	81.8	3	—	—	—	—	—
SK42#1	—	86	11	—	3	—	—	—
SK42#2	41	52	—	4	3	—	—	—
SK43#1	46	52	—	—	—	—	2	—
SK43#2	49	44	—	—	—	5	2	—

4.4. Analysis of Differences in Coalbed Gas Content and Control Factors

4.4.1. Coalbed gas content

Coal reservoir gas content refers to the amount of gas contained per unit mass of coal, and is the most direct parameter for characterizing the gas content [44], and is regarded as a key parameter affecting the development potential of CBM resources. Estimates of the gas content of drill cores measured by a field desorption method indicates that the gas content in the main coal seams of No. 10 coal mine are as follows: for SK21 it is 0.37–3.73 m^3t^{-1} (average 2.27 m^3t^{-1}); for SK42 it is 6.49–8.61 m^3t^{-1} (average 7.39 m^3t^{-1}); and for SK43 it is 7.03 m^3t^{-1} (Table 5). It is seen that the gas content of SK42 and SK43 is relatively high, and for SK21 coal seam it is obviously low.

Table 5. Measurement results of CBM content and gas fraction of SK21, SK42 and SK43 samples (Own work).

Sample ID	Depth/m	Total gas content (daf) / $m^3 \cdot t^{-1}$	Methane content (daf) / $m^3 \cdot t^{-1}$	Gas composition/ % (Normalized after deducting air)				Adsorption time/d
				CH_4	CO_2	N_2	C_2H_6	
SK21#1	872.22-872.52	2.08	1.16	55.94	4.72	37.72	1.62	3.46
SK21#2	873.43-873.73	3.73	2.88	77.25	10.51	9.49	2.75	1.30
SK21#3	874.73-875.03	2.85	2.29	80.30	8.70	8.06	2.94	1.54
SK21#4	875.73-876.03	3.01	2.48	82.22	9.30	4.79	3.70	0.94
SK21#5	876.68-876.98	1.58	0.75	47.50	4.26	46.23	2.01	0.98
SK21#6	877.69-877.99	0.37	0.20	55.20	2.59	40.70	1.51	0.29
SK42#1	699.36-699.66	7.07	6.64	93.99	1.18	4.81	0.02	4.26
SK42#2	699.99-700.29	8.61	8.19	95.16	0.97	3.85	0.01	3.19
SK42#3	701.00-701.30	6.49	5.99	92.32	0.97	6.69	0.02	3.07
SK43#1	692.02-692.32	7.03	6.60	93.89	1.62	4.47	0.02	2.73

 doi:10.20944/preprints202310.1832.v1

Analysis of the gases from each coal seam after deducting the air content showed that methane was the dominant gas component, followed by nitrogen, a small amount of carbon dioxide and trace amounts of ethane. The methane content in SK21 is 47.50–82.22% (average 66.40%); for SK42 it is 92.32–95.16% (average 93.82%); and in SK43 it is 93.89%. The gas content and methane purity of SK42 and SK43 are significantly higher than in SK21, and have better development potential. Although the maximum methane adsorption of the SK21 samples is obviously larger than for SK42 and SK43, their gas content is about three times that of SK21. The following reasons were inferred from the above experiments.

4.4.2. The influence of coal seam thickness and depth

Coal seam thickness, depth of burial, reservoir pressure and temperature, surrounding rock porosity, permeability and hydrogeological conditions all affect the gas content of coal [45–48]. On average, SK43 is 1.02 m thick, SK42 it is 4.23 m thick, and SK21 is 3.44 m. The similar thicknesses of the three coal seams had little effect on gas content. The gas content of the coal in the study area is positively correlated with burial depth, with the exception of SK21, which is deeper than SK42 and SK43 but clearly contains less gas.

4.4.3. The influence of coal seam roof and floor lithology

The sealing ability of the roof and floor of coal seams is one of the factors affecting CBM content [49]. Poor roof and floor sealing conditions and their permeability lead to easy gas dispersion from the coal, resulting in low content; poor gas permeability of the surrounding rock is conducive to the preservation of gas, and thus high CBM content. The roof rock of the SK21 seam is sandy mudstone interbedded with thinly bedded sandstone; the floor rock is a scaly muscovitic sandy mudstone overlying tuff, and the middle of the seam is poorly sealed and extremely soft, none of which is conducive to the storage of CBM. This may be the reason why the theoretical saturated adsorption capacity of the SK21 coal seam is high but the actual gas content is low. The roof rock of the SK42 and SK43 coal seams is mostly mudstone and sandy mudstone, and the floor rock is sandy mudstone. Both of these materials are reasonably impermeable, which favors CBM storage.

4.4.4. Characterization of the organic microcomponents of coal

The vitrinite and inertinite content in coal has an obvious influence on the development of coal porosity; in addition, micropores in the vitrinite promotes the adsorption capacity of the coal, and most of the gases in the coal may be adsorbed in the micropores [50–52]. In the present study, it was found that the porosity of SK21 was 39.34%, whereas the values for SK42 and SK43 were 4.98–5.17% and 5.78–8.08%, respectively. Despite the very much larger porosity of the SK21 coal, the distributions of pore diameters in the three SK21 samples were similar to those of the SK42 and SK43 samples. Obviously, while the greater storage space of the SK21 coal allows for more adsorbed gas, the gas is dispersed into the sandy mudstone; Therefore, it is recommended that the coal seam and the mudstone be exploited jointly.

4.4.5. The influence of mineral characteristics

Clay containing minerals such as kaolinite and quartz may fill primary and secondary pore spaces leading to a significant reduction in reservoir porosity, and is the main influence on the evolution of reservoir quality [53–57]. Kaolinite fills the pore space and also plugs the pore throat, significantly lowering reservoir permeability and gas saturation [58]. Considering that biogenic quartz protects rather than destroys pores [59], the high kaolinite and low quartz content of the SK21 seam are the result of its high porosity.

4.5. Challenges and prospects

This study has obtained a relatively systematic theory, which provides theoretical support for gas content prediction, optimization of drilling location and finding out "sweet spot" and so on, and

 doi:10.20944/preprints202310.1832.v1

has very important practical significance for the development of CBM on site. However, due to the complexity of the geological conditions of coal reservoirs, the gas bearing properties of coal seams in different regions are very different. Through the study of the physical characteristics of coal reservoirs in Pingdingshan No 10 Mine, HPMI and SEM are difficult to fully characterize the pore-fracture characteristics of coal. Therefore, CO_2 adsorption, Low temperature liquid nitrogen adsorption, CT scanning and HPMI combined analysis should be added to the research on the reservoir characteristics of CBM Wells. For the characterization of full aperture and structure. In addition, the gas content of coal seam is controlled by many factors, however, the strength of the combined influence of a single factor and a variety of factors, and the quantitative relationship between different factors need to be further studied.

5. Conclusion

In this paper, the gas properties, adsorption properties, pore and fracture characteristics and mineral characteristics of 5 groups of samples from No. 2 and No. 4 coal seam of Pingdingshan No. 10 coal mine were characterized by field analysis, isothermal adsorption, HPMI, XRD and SEM, and the following conclusions were drawn:

1. The average gas content of SK21 was 2.27 m^3t^{-1}; the average gas content of SK42 was 7.39 m^3t^{-1}; and the average gas content of SK43 was 7.03 m^3t^{-1}. Thus the gas content of SK42 and SK43 in the No. 10 Mine Field was relatively high, and was obviously low for SK21. Moreover, the gas content and methane purity of the No. 4 coal seam were significantly higher than the No. 2 seam, and therefore they have better development potential than the No. 2 seam.
2. Isothermal adsorption experiments indicate that the theoretical saturated adsorption amount of methane in the No. 4 coal seam was slightly below that of the No. 2 seam. The average adsorption time of the No. 2 coal seam was less than that of the No. 4 seam, and the adsorption time was shorter, making it easier to reach the peak production capacity of CBM wells in the short term, but was not conducive to long-term stable production of CBM. The adsorption curves indicate that the Langmuir volume of the No. 2 coal seam samples was significantly greater than for the No. 4 coal seam; however, the No. 4 coal seam contains about three times the amount of gas in the No. 2 seam.
3. All three coal seams have high porosity, which was favorable for large amounts of CBM adsorption and storage. Micropores predominate, transitional pores were less frequent, and a few mesopores occur; macropores were the least common. Samples from the No. 4 seam contained the highest proportion of micropores.
4. Organic pores were common in the coal samples, with pore diameters not more than 30 μm, mainly concentrated between 50.5 and 1000 nm. Intergranular and intragranular pores were observed in inorganic minerals; a considerable proportion of the intergranular pores were filled with clay minerals. Microfractures with apertures less than 70 nm were relatively frequent, mainly in the 50–65 nm range. A large number of the nanoscale microfractures were curved or jagged.
5. Fractures in the No. 2 and No. 4 coal seam samples with widths of 50 nm to 20 μm were more developed, and many were filled with kaolinite, quartz and other minerals; some of the filled fractures were spaced at the nanometer level, between 50 and 800 nm. The maximum open fracture aperture was not more than 2 μm, with the minimum averaging around 62 nm. These were relatively simple in shape, with a hundred to several hundreds often occurring in the one place.
6. The samples contained mostly layered silicate minerals (kaolinite), with hard granular minerals (quartz) next, and a very small quantity of iron-type minerals such as siderite and pyrite in dendritic form.

References

1. Raza, S.; Orooji, Y.; Ghasali, E.; et al. Engineering approaches for CO_2 converting to biomass coupled with nanobiomaterials as biomediated towards circular bioeconomy. *Journal of CO_2 Utilization.* **2023**, 67: 102295.
2. Raza, S.; Ghasali, E.; Orooji, Y.; et al. Two dimensional (2D) materials and biomaterials for water desalination; structure, properties, and recent advances. *Environmental Research.* **2022**: 114998.

3. Wang, X.; Pan, J.; Wang, K.; et al. Fracture variation in high-rank coal induced by hydraulic fracturing using X-ray computer tomography and digital volume correlation. *International Journal of coal geology.* **2022**, 252: 103942.
4. Prabu, V.; Mallick, N. Coalbed methane with CO_2 sequestration: An emerging clean coal technology in India. *Renewable and Sustainable Energy Reviews.* **2015**, 50: 229-244.
5. Teng, T.; Gao, F.; Ju, Y.; et al. How moisture loss affects coal porosity and permeability during gas recovery in wet reservoirs. *International Journal of Mining Science and Technology* .**2017**, 27(6): 899-906.
6. Wen, S.; Zhou, K.; Lu, Q. A discussion on CBM development strategies in China: A case study of PetroChina Coalbed Methane Co., Ltd. *Natural Gas Industry B* .**2019**, 6(6): 610-618.
7. Raza, S.; Ghasali, E.; Raza, M.; et al. Advances in technology and utilization of natural resources for achieving carbon neutrality and a sustainable solution to neutral environment. *Environmental Research.* **2022**: 115135.
8. Liu, D.; Jia, Q.; Cai, Y.; et al. A new insight into coalbed methane occurrence and accumulation in the Qinshui Basin, China. *Gondwana Research.* **2022**, 111: 280-297.
9. Gao, C.; Liu, D.; Vandeginste, V.; et al. Thermodynamic energy change and occurrence mechanism of multiple fluids in coal reservoirs. *Energy* **2023**, 283: 129089.
10. Fu, X.; Qin, Y.; Wang, G G X.; et al. Evaluation of gas content of coalbed methane reservoirs with the aid of geophysical logging technology. *Fuel* **2009**, 88(11): 2269-2277.
11. Wang, S.; Elsworth, D.; Liu, J. Permeability evolution in fractured coal: the roles of fracture geometry and water-content. *International Journal of Coal Geology* .**2011**, 87(1): 13-25.
12. Weniger, S.; Weniger, P.; Littke, R. Characterizing coal cleats from optical measurements for CBM evaluation. *International Journal of Coal Geology*,.**2016**, 154: 176-192.
13. Wang, X.; Pan, J.; Deng, Z.; et al. Comparison of fracture and permeability between tectonically deformed coal and briquette coal using x-ray computer tomography and the lattice Boltzmann method. *Natural Resources Research.* **2023**, 32(5): 2223-2241.
14. Diamond, W, P.; Schatzel, S J. Measuring the gas content of coal: A review. International Journal of Coal Geology. **1998**, 35(1-4): 311-331.
15. Wang, L.; Cheng, L.; Cheng, Y.; et al. A new method for accurate and rapid measurement of underground coal seam gas content. Journal of Natural Gas Science and Engineering. **2015**, 26: 1388-1398.
16. Wang, X.; Pan, J.; Wang, K.; et al. Characterizing the shape, size, and distribution heterogeneity of pore-fractures in high rank coal based on X-ray CT image analysis and mercury intrusion porosimetry. *Fuel* ***2020***, 282: 118754.
17. Zhang, J.; Wei, C.; Ju, W.; et al. Stress sensitivity characterization and heterogeneous variation of the pore-fracture system in middle-high rank coals reservoir based on NMR experiments. Fuel **2019**, 238: 331-344.
18. Ramandi, H L.; Mostaghimi, P.; Armstrong, R T.; et al. Porosity and permeability characterization of coal: a micro-computed tomography study. *International Journal of Coal Geology*. **2016**, 154: 57-68.
19. Karacan, C O.; Okandan, E. Adsorption and gas transport in coal microstructure: investigation and evaluation by quantitative X-ray CT imaging. *Fuel* **2001**, 80(4): 509-520.
20. Giffin, S.; Littke, R.; Klaver, J.; et al. Application of BIB–SEM technology to characterize macropore morphology in coal. *International Journal of Coal Geology*. **2013**, 114: 85-95.
21. Zhou, S.; Yan, G.; Xue, H.; et al. 2D and 3D nanopore characterization of gas shale in Longmaxi formation based on FIB-SEM. *Marine and Petroleum Geology*. **2016**, 73: 174-180.
22. Zelenka, T. Adsorption and desorption of nitrogen at 77 K on micro-and meso-porous materials: Study of transport kinetics. *Microporous and Mesoporous Materials.* **2016**, 227: 202-209.
23. Raut, U.; Famá, M.; Teolis, B D.; et al. Characterization of porosity in vapor-deposited amorphous solid water from methane adsorption. *The Journal of chemical physics*. **2007**, 127(20).
24. Chalmers, G R L.; Bustin, R M. Lower Cretaceous gas shales in northeastern British Columbia, Part I: geological controls on methane sorption capacity. *Bulletin of Canadian petroleum geology*. **2008**, 56(1): 1-21.
25. Wang, Z.; Fu, X.; Pan, J.; et al. Effect of N_2/CO_2 injection and alternate injection on volume swelling/shrinkage strain of coal. *Energy* **2023**, 275: 127377.
26. Sarrazin, P.; Blake, D.; Feldman, S.; et al. Field deployment of a portable X-ray diffraction/X-ray flourescence instrument on Mars analog terrain. *Powder Diffraction*. **2005**, 20(2): 128-133.
27. Guo, S. Experimental study on isothermal adsorption of methane gas on three shale samples from Upper Paleozoic strata of the Ordos Basin. *Journal of Petroleum Science and Engineering*. **2013**, 110: 132-138.
28. Su, X B.; Zhang, L P.; Lin, X Y. Influence of coal rank on coal adsorption capacity. *Natural Gas Industry*. **2005**, 25(1): 19-21.
29. Gao, Z.; Liang, Z.; Hu, Q.; et al. A new and integrated imaging and compositional method to investigate the contributions of organic matter and inorganic minerals to the pore spaces of lacustrine shale in China. *Marine and Petroleum Geology*. **2021**, 127: 104962.
30. Roslin, A.; Pokrajac, D.; Wu, K.; et al. 3D pore system reconstruction using nano-scale 2D SEM images and pore size distribution analysis for intermediate rank coal matrix. *Fuel* **2020**, 275: 117934.

31. Moore, T A. Coalbed methane: A review. *International Journal of Coal Geology*. **2012**, 101: 36-81.
32. Liu, W.; Wang, G.; Han, D.; et al. Accurate characterization of coal pore and fracture structure based on CT 3D reconstruction and NMR. *Journal of Natural Gas Science and Engineering*. **2021**, 96: 104242.
33. Loucks, R G.; Reed, R M.; Ruppel, S C.; et al. Morphology, genesis, and distribution of nanometer-scale pores in siliceous mudstones of the Mississippian Barnett Shale. *Journal of sedimentary research*. **2009**, 79(12): 848-861.
34. Schieber, J. Common themes in the formation and preservation of intrinsic porosity in shales and mudstones–illustrated with examples across the Phanerozoic. *SPE Unconventional Gas Conference. OnePetro* **2010**.
35. Zhang, H.; Jin, X.; Wu, J.; et al. Nano-pores of organic matter in Longmaxi Formation shale in Sichuan Basin. *Coal Geology & Exploration*. **2018**, 46(3): 47-53.
36. Zhang, J.; Wang, H.; Vandeginste, V.; et al. Effect of litho-facies on nano-pore structure of continental shale in shuinan formation of Jiaolai Basin. *Geoenergy Science and Engineering*. **2023**: 212020.
37. Juan, W.; Wei, W.; Xue-feng, H.; et al. Micropore structure characteristics of shale in the Paleogene Sha-4 Member, Dongying Sag. *Journal of electron microscopy*. **2017**, 36(4): 368-375.
38. Yu, B S. Classification and characterization of gas shale pore system. *Earth Science Frontiers*. **2013**, 20(4): 211-220.
39. Qin, S.; Wang, R.; Shi, W.; et al. Diverse effects of intragranular fractures on reservoir properties, diagenesis, and gas migration: Insight from Permian tight sandstone in the Hangjinqi area, north Ordos Basin. *Marine and Petroleum Geology*. **2022**, 137: 105526.
40. Wang, Y.; Zhu, Y.; Liu, S.; et al. Pore characterization and its impact on methane adsorption capacity for organic-rich marine shales. *Fuel* **2016**, 181: 227-237.
41. Jinling, L. The Analysis of Coal Reservoir Physical Propertiesand Geological Factors in Southern Qinshui Basin. **2011**, China University of Geosciences (Beijing).
42. Guihong, L I.; Zhang, H.; Zhang, H.; et al. Characteristics of fractures and pores of anthracite in Jincheng by SEM. *Mining Science and Technology (China)*. **2010**, 20(5): 789-793.
43. Liu, Y.; Liu, A.; Liu, S.; et al. Nano-scale mechanical properties of constituent minerals in shales investigated by combined nanoindentation statistical analyses and SEM-EDS-XRD techniques. *International Journal of Rock Mechanics and Mining Sciences*. **2022**, 159: 105187.
44. Li, J.; Lu, S.; Zhang, P.; et al. Estimation of gas-in-place content in coal and shale reservoirs: A process analysis method and its preliminary application. *Fuel* **2020**, 259: 116266.
45. Song, L I.; Dazhen, T.; Hao, X U.; et al. Progress in geological researches on the deep coalbed methane reservoirs. *Earth Science Frontiers*. **2016**, 23(3): 10.
46. Meng, Y.; Li, Z. Experimental study on diffusion property of methane gas in coal and its influencing factors. *Fuel* **2016**, 185: 219-228.
47. Meng, Z.; Yan, J.; Li, G. Controls on gas content and carbon isotopic abundance of methane in Qinnan-East coal bed methane block, Qinshui Basin, China. *Energy & Fuels*. **2017**, 31(2): 1502-1511.
48. Wei, Q.; Li, X.; Hu, B.; et al. Reservoir characteristics and coalbed methane resource evaluation of deep-buried coals: A case study of the No. 13–1 coal seam from the Panji Deep Area in Huainan Coalfield, Southern North China. *Journal of Petroleum Science and Engineering*. **2019**, 179: 867-884.
49. Cai, Y.; Liu, D.; Zhang, K.; et al. Preliminary evaluation of gas content of the No. 2 coal seam in the Yanchuannan area, southeast Ordos basin, China. *Journal of Petroleum Science and Engineering*. **2014**, 122: 675-689.
50. Fu, S.; Wang, L.; Li, S.; et al. The effect of organic matter fraction extracted on micropores development degree and CH_4 adsorption capacity of coal. *Gas Science and Engineering*. **2023**, 110: 204870.
51. Song, D.; Ji, X.; Li, Y.; et al. Heterogeneous development of micropores in medium-high rank coal and its relationship with adsorption capacity. *International Journal of Coal Geology*. **2020**, 226: 103497.
52. Wang, Z.; Hao, C.; Wang, X.; et al. Effects of micro-mesopore structure characteristics on methane adsorption capacity of medium rank coal. *Fuel* **2023**, 351: 128910.
53. Guanghui, Y.; Yingchang, C A O.; Kelai, X I.; et al. Feldspar dissolution and its impact on physical properties of Paleogene clastic reservoirs in the northern slope zone of the Dongying sag. *Acta Petrolei Sinica*. **2013**, 34(5): 853.
54. Yuan, G.; Cao, Y.; Gluyas, J.; et al. Feldspar dissolution, authigenic clays, and quartz cements in open and closed sandstone geochemical systems during diagenesis: Typical examples from two sags in Bohai Bay Basin, East China. *AAPG Bulletin*. **2015**, 99(11): 2121-2154.
55. Ma, B.; Lu, Y.; Eriksson, K A.; et al. Multiple organic–inorganic interactions and influences on heterogeneous carbonate-cementation patterns: Example from Silurian deeply buried sandstones, central Tarim Basin, north-western China. *Sedimentology*. **2021**, 68(2): 670-696.
56. Gao, Y.; Wang, Z.; She, Y.; et al. Mineral characteristic of rocks and its impact on the reservoir quality of He 8 tight sandstone of Tianhuan area, Ordos Basin, China. *Journal of Natural Gas Geoscience*. **2019**, 4(4): 205-214.

57. Jiu, B.; Huang, W.; Li, Y.; et al. Influence of clay minerals and cementation on pore throat of tight sandstone gas reservoir in the eastern Ordos Basin, China. *Journal of Natural Gas Science and Engineering*. **2021**, 87: 103762.
58. Lai, J.; Wang, G.; Cao, J.; et al. Investigation of pore structure and petrophysical property in tight sandstones. *Marine and Petroleum Geology*. **2018**, 91: 179-189.
59. Ye, Y.; Tang, S.; Xi, Z.; et al. Quartz types in the Wufeng-Longmaxi Formations in southern China: Implications for porosity evolution and shale brittleness. *Marine and Petroleum Geology*. **2022**, 137: 105479.